Design of UWB Antennas to Monitor Cardiac Activity

Erika Pittella, Paolo Bernardi, Marta Cavagnaro, Stefano Pisa, and Emanuele Piuzzi

Department of Information Engineering, Electronics, and Telecommunications
Sapienza University of Rome, Rome, Italy
pisa@die.uniroma1.it

Abstract ─ This paper presents two novel ultra wideband (UWB) printed antennas designed to be part of a UWB radar system for cardiac activity monitoring. The two antennas have the same shape but differ in terms of dielectric substrate and dimensions and are designed to be used one in a wearable and the other in non-wearable (fixed) radar. With regard to the fixed antenna, numerical results show an optimum fidelity factor and an almost constant group delay in the 3.1 - 10.6 GHz frequency band. As concerns the wearable antenna, numerical results obtained considering the antenna placed in the vicinity of a box model of the thorax, containing a spherical model of the heart, show that small heart movements can be detected. Eventually, the two antennas have been realized and measured by means of a vector network analyzer finding a return loss lower than -10 dB in the 3.1 - 10.6 GHz frequency band with a good agreement between simulations and measurements. Also, measurements of the fixed antenna gain and radiation pattern, performed in an anechoic chamber, show a good agreement with simulations.

Index Terms ─ Heart-activity monitoring, remote sensing, UWB antenna.

I. INTRODUCTION

The cardiac activity involves changes in shape, dimension, and dielectric properties of the heart muscle. These variations can be monitored by using a UWB radar system equipped with a suitable antenna. In a possible arrangement, the radar transmits very short pulses towards the human thorax and receives the echoes containing information on the heart variations [1, 2]. The remote monitoring of cardiac activity is a crucial and useful application in various situations. For example, in emergency rooms or intensive care units it is more comfortable for the patient with respect to conventional techniques (e.g., electrocardiogram - ECG). Moreover, it can be performed in a continuous way, becoming very useful in the monitoring of pathologies of the cardiac apparatus, for home therapy, or hospital confinement. Finally, it allows monitoring of patients with burns or chemical contaminations without contacting electrodes.

With reference to UWB radar systems, their main advantages are the very high resolution, the low power spectral density, and the low electromagnetic interference with other systems; furthermore, UWB radars are based on a quite low cost technology. In February 2002, the Federal Communications Commission (FCC) gave the permission for the development of new products incorporating UWB technology. To this day, the FCC allocated a 7.5 GHz band in the range from 3.1 GHz to 10.6 GHz [3, 4] providing a mask for the maximum power spectral density (PSD), settled to the value of -41.3 dBm/MHz, over the whole band. These low levels are due to the fact that UWB systems work in a region of the spectrum in which other services already operate. UWB radar systems can be realized in hybrid or monolithic microwave integrated circuit (MMIC) technology with very small dimensions so that portable (wearable) radars can be built. Otherwise, in many applications, the dimensions are not a strong constrain and the radar can be fixed on the roof or on a wall of a room. These two

applications will need antennas with different dimensions and properties.

For this reason, in this work, two novel UWB antennas have been proposed and designed, one for wearable and one for fixed radars.

II. ANTENNAS DESIGN

A. Antenna geometry

The main goal of the two antenna designs is to obtain a return loss lower than -10 dB in the 3.1 - 10.6 GHz band. Moreover, the wearable antenna has to be portable and light while for the fixed one the directivity constrain is more important. To fulfill these requirements, printed UWB antennas can be used [5-11]. In particular, among these antennas, the microstrip-fed monopole structure has been considered, where the radiating element and the feeding microstrip line are realized over one of the substrate faces, while a suitable ground plane is etched on the other face. Such structure has been chosen considering the broadband and good radiation properties of the printed heart monopole antenna [5]. Finally, taking into account the directivity performance of the truncated planar configuration proposed in [12], a half-heart shape geometry has been chosen.

B. Antenna optimization

The considered half-heart shape geometry is shown in Fig. 1. The radiator is located on the top layer of the substrate and the ground plane on the bottom layer. The dielectric substrates utilized in this project are: Rogers RO4003 with relative permittivity ε_{r1} = 3.38, thickness h_1 = 0.508 mm, and copper thickness t_1 = 0.035 mm, and Rogers RT6010 with ε_{r2} = 10.2, thickness h_2 = 0.640 mm, and copper thickness t_2 = 0.035 mm, for the antenna to be used in fixed and wearable systems, respectively. With reference to the other dimensions, l and w are the height and width of the substrate. The shape of the half heart on the top layer is obtained through a semicircle of radius r_c and through a three control-points spline defined assigning the initial point $P_i(x_i,y_i,z_i)$, the final point $P_f(x_f,y_f,z_f)$, and the central point $P_s(x_s,y_s,z_s)$. The shape of the ground on the bottom layer of the antenna is also obtained through a three control-points spline specular to the previous one (see Fig. 1). It is worth noting that, in all the simulations, the feeding microstrip line has been curved away from the edge of the structure to facilitate the connection with the coaxial feed line.

The antenna geometry has been optimized through parametric simulations using CST Microwave Studio® software [13]. In these simulations the antenna parameters have been varied inside realistic ranges and the $S_{11}(f)$ results

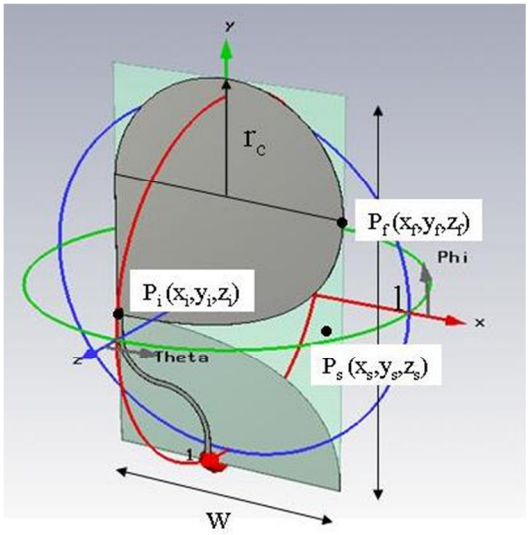

Fig. 1. Geometry of the proposed antenna.

have been analyzed. Only geometries giving $S_{11}(f)$ absolute values lower than -10 dB (ρ = 0.316) between f_1 = 3.1 GHz and f_2 =10.6 GHz band have been considered and, among those selected, the one maximizing the cost function:

$$C = \frac{1}{(f_2 - f_1)} \int_{f_1}^{f_2} \left(\frac{\rho - |S_{11}(f)|}{\rho} \right) df, \qquad (1)$$

has been chosen.

Among the antenna parameters, the central control-point of the spline (x_s, y_s) plays a fundamental role for the antenna matching. This parameter has been varied at 1 mm step in the 10-50 mm range. Figure 2 shows the results for l = 85 mm, w = 50 mm, r_c = 25 mm, x_s = 50 mm and for three values of the y_s parameter.

The best value of the cost function is obtained with y_s = 30 mm and corresponds to C = 0.633.

The final antenna dimensions are: l_1 = 85.0 mm, w_1 = 50 mm, r_{c1} = 25 mm, x_{s1} = 50 mm, y_{s1} = 30 mm for the fixed antenna, and l_2 = 48.5 mm, w_2 = 25 mm, r_{c2} = 12.5 mm, x_{s2} = 25 mm, y_{s2} = 20 mm for the wearable one.

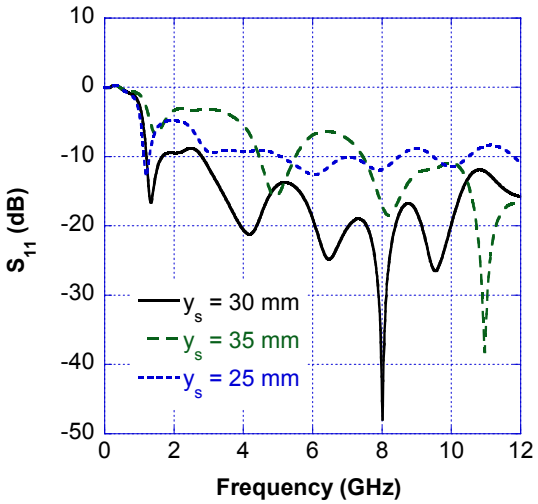

Fig. 2. Results of a parametric analysis.

III. NUMERICAL SIMULATION RESULTS

A. Antennas performances in free space

Figure 3 shows the return loss as a function of the frequency for the two designed UWB antennas. The obtained results indicate that the antennas have a return loss below -10 dB in the 3.1-10.6 GHz frequency band.

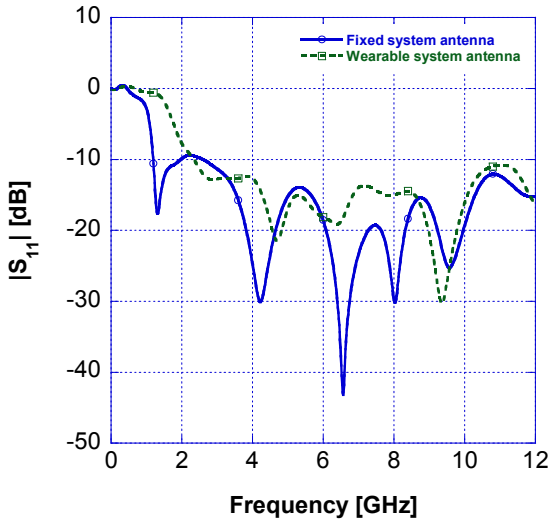

Fig. 3. Return loss of the two proposed antennas.

B. Fixed system antenna

Concerning the antenna radiation pattern, Fig. 4 shows polar plots on the x-y vertical plane at 4, 6, 8, and 10 GHz for the antenna designed for the fixed system. The plot highlights that the direction of maximum radiation is close to the x direction of Fig. 1 with a -3 dB aperture varying between 55° and 58.5°.

Figure 5 shows the peak gain behavior as a function of the frequency as well as the φ value ($\theta = 90°$) for which the gain achieves its maximum value. As it can be seen, the gain values increase with the frequency. In particular, the minimum value is 4.6 dBi at 3.0 GHz, while the maximum is 9.4 dBi at 11 GHz; these gain values are comparable with the gain values of other UWB antennas reported in literature [8].

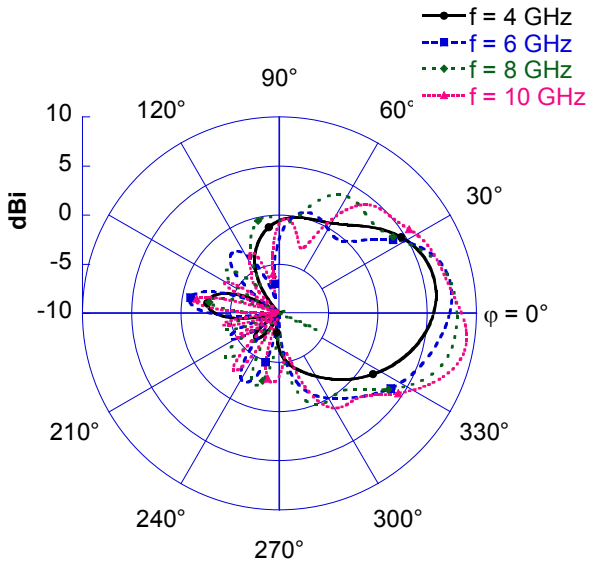

Fig. 4. Polar plot of the gain at 8 GHz for the fixed antenna.

Concerning the direction of maximum radiation, Fig. 5 shows that it is almost constant with the frequency with variations mostly within ± 10 °.

An important parameter of a UWB antenna is the fidelity factor that is the peak value of the cross correlation function between the observed pulse $s_2(t)$ (electric field (E_θ)), at a given distance from the antenna, and the excited pulse $s_1(t)$ (input voltage) [14, 15]:

$$F = \max_{\tau} \frac{\int_{-\infty}^{+\infty} s_1(t)\, s_2(t+\tau)dt}{\sqrt{\int_{-\infty}^{+\infty} s_1^2(t)dt}\sqrt{\int_{-\infty}^{+\infty} s_2^2(t)dt}}, \qquad (2)$$

where τ is the delay that maximizes F in (2). Considering that, for an antenna, the time behavior of the radiated electric field is an approximation of the derivative of the input excitation,

$s_1'(t) = ds_1 / dt$ can be used in place of $s_1(t)$ [14]. The UWB signal used in [14, 16] is assumed to excite the designed antenna. This UWB signal is the 5th-derivative of the Gaussian pulse, given by:

$$s_1(t) = k\left(-\frac{t^5}{\sqrt{2\pi}\sigma^{11}} + \frac{10t^3}{\sqrt{2\pi}\sigma^{9}} - \frac{15t}{\sqrt{2\pi}\sigma^{7}}\right)e^{\left(-\frac{t^2}{2\sigma^2}\right)}, \quad (3)$$

where k is a constant which can be chosen to comply with the peak power spectral density allowed by the FCC, while σ is taken equal to 51 ps to ensure that the spectrum shape complies with the FCC spectral mask.The fidelity factor has been calculated at a distance from the antenna of 100 cm and for various directions. Results concerning the fidelity ($s_1(t)$ and its derivative) are summarized in Tab. 1. The values reported in the table highlight a very high fidelity factor of the proposed antenna, for all the considered directions apart from small θ angles.

Another important goal of the UWB antenna design is to achieve a linear dependence of the radiated field phase as a function of the frequency in order to minimize pulse distortion. The parameter that describes the phase response of the antenna is the group delay, defined as the negative derivative of the phase response with respect to the frequency. Figure 6 shows the group delay values as calculated from the time-domain response. The figure reveals that the antenna group delay is almost constant, with less than 0.1 ns fluctuations, across the whole considered frequency band.

C. Wearable antenna in the presence of a box model of the thorax

In order to check the ability of the wearable antenna to monitor the heart activity, the radiating structure has been placed 1 cm from a box model of the chest (9×9×6 cm) with the direction of maximum radiation toward the thorax (see Fig. 7).

Inside the box, at a depth of 3 centimeters, a sphere of variable radius (from 20 to 25 mm) has been placed to simulate the presence of the heart.

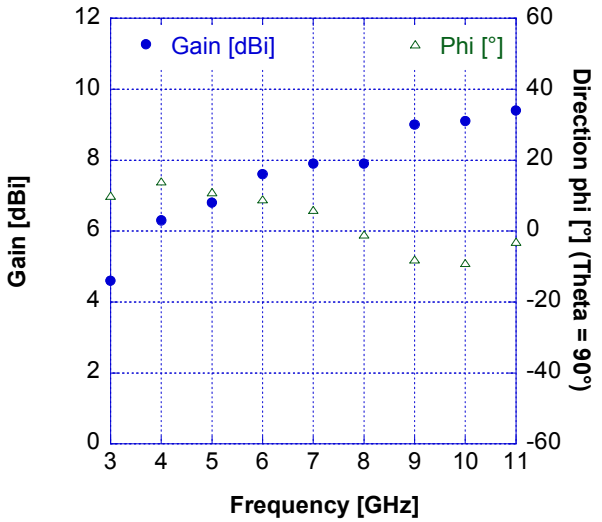

Fig. 5. Peak gain behavior of the fixed system antenna and direction of maximum gain as a function of the frequency.

The thorax is constituted by an equivalent body tissue whose parameters have been taken from those recommended by the IEEE SCC-34/SC-2 [17]. The values in [17] have been interpolated by using a Cole-Cole equation [18] with ε_s= 993, ε_∞= 54, and relaxation frequency f_r = 20.8 MHz. For the sphere representing the heart, ε_r = 48.62 and σ = 6.12 S/m [19, 20] have been considered.

To simulate the heart movements, a set of simulations have been performed varying the sphere radius and measuring the received voltage at the feed point considering as a source signal the 5th derivative of the Gaussian pulse.

Table 1. Simulated fidelity of the proposed antenna.

	Probe position (xy plane)	Fidelity $s_1(t)$	Fidelity $s_1'(t) = ds_1 / dt$	Probe position (xz plane)	Fidelity $s_1(t)$	Fidelity $s_1'(t) = ds_1 / dt$
Antenna (fixed system)	$\theta = 90°$ $\varphi = 0°$	0.947	0.983	$\varphi = 0°$ $\theta = 0°$	0.700	0.706
	$\theta = 90°$ $\varphi = 30°$	0.961	0.964	$\varphi = 0°$ $\theta = 30°$	0.825	0.767
	$\theta = 90°$ $\varphi = 60°$	0.964	0.975	$\varphi = 0°$ $\theta = 60°$	0.948	0.964
	$\theta = 90°$ $\varphi = 90°$	0.925	0.928	$\varphi = 0°$ $\theta = 90°$	0.925	0.983

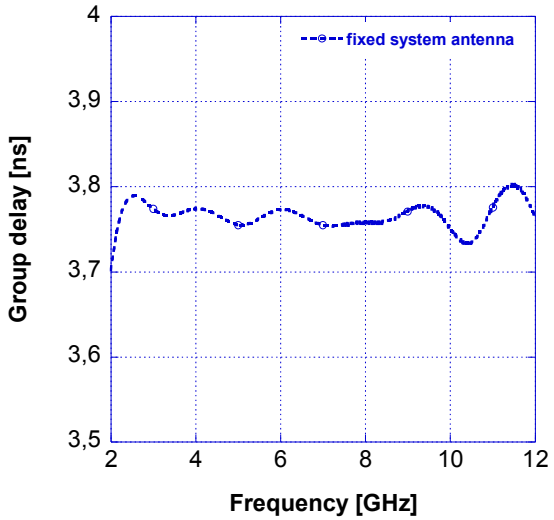

Fig. 6. Group delay of the proposed fixed system antenna.

Since the early time contents of this signal are dominated by the antenna and skin reflection, a calibration procedure has been implemented. The calibration signal has been calculated as the average value of all the measured voltages and has been subtracted from each received signal thus obtaining the calibrated signals. Figure 8 shows the calibrated signals corresponding to the minimum and maximum sphere radius, i.e. 2 cm and 2.5 cm respectively, simulating the end-systole and the end-diastole conditions.

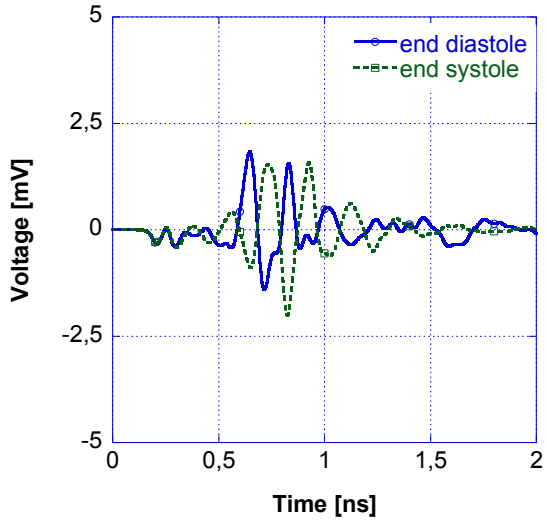

Fig. 8. Received signals for two cardiac phases.

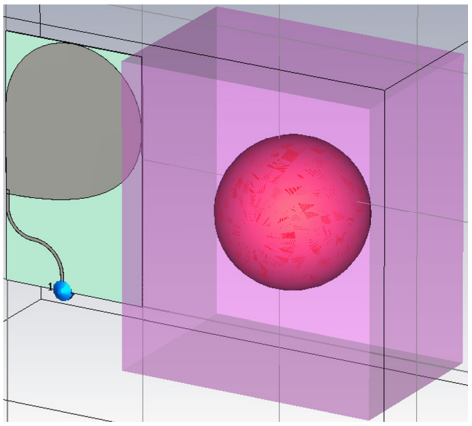

Fig. 7. Antenna in the presence of biological tissues.

The figure highlights that it is possible to distinguish between the two positions; in fact the corresponding signals arrive at the antenna feed point at different time instants (about 120 ps distance between the absolute minimum of the two signals) and, consequently, the heart movements can be detected through a suitable radar receiver.

IV. MEASUREMENT RESULTS

The two UWB antennas have been realized using a milling table and a SMA connector has been soldered at the input of the microstrip line. The photograph of the manufactured antennas including the coaxial connector is shown in Fig. 9.

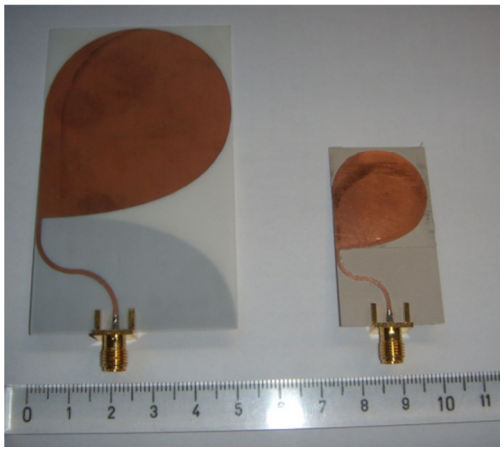

Fig. 9. Realized UWB antennas.

Return loss measurements were performed using a PNA E8363B network analyzer and placing the antenna in an anechoic chamber.

The measured return loss for the fixed antenna printed on RO4003 is reported in Fig. 10 indicating that the antenna features UWB behavior with a bandwidth from 3.1 GHz to more than 10.6 GHz assuming a -10 dB return loss reference. On the same figure, simulation results obtained adding the SMA connector to the antenna is also reported. A good agreement between numerical and experimental results is obtained. However, comparing Fig. 10 with Fig. 3 it can be noted that the presence of the connector makes the antenna return loss worse.

With reference to the wearable antenna, both simulations and measurements (not shown) have evidenced that, also in this case, the presence of the connector makes the return loss worse than the one obtained without the connector.

Since, in the final radar layout, the wearable antenna will be directly connected to a microstrip circuit, i.e. without a coaxial connector, the time domain reflectometry (TDR) technique has been used to remove, by means of the gating function, the connector effect from the measured data [21].

The obtained results are shown in Fig. 11, where the TDR measurements are compared with the simulations in the absence of the connector. The figure shows a good agreement between simulations and measurements especially in the 3.1 - 10.6 GHz frequency band.

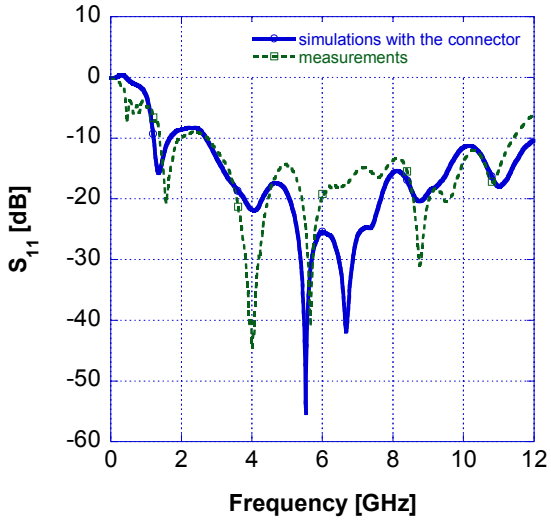

Fig. 10. Comparison between simulations and measurements for the fixed system antenna.

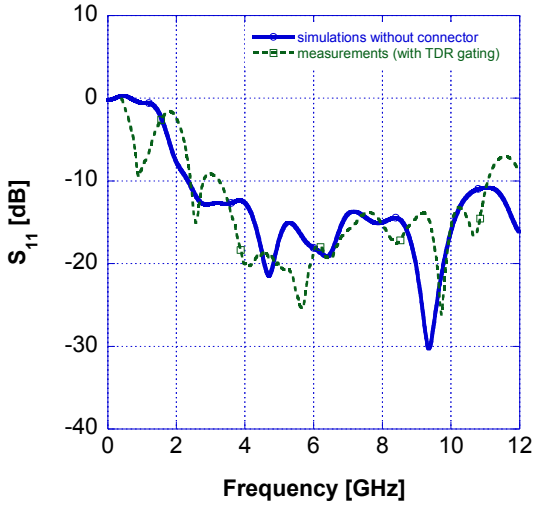

Fig. 11. Comparison between simulations and measurements for the wearable system antenna.

The fixed antenna has been further characterized by measuring the gain for a given direction ($\theta = 90°$, $\varphi = 0°$). This has been done by using the anechoic chamber available at ENEA-Casaccia research center and by using the gain transfer technique [22]. Figure 12 shows a comparison between measured and simulated values. Taking into account the measurement uncertainty of ± 2 dB the measurements are in good agreement with simulations.

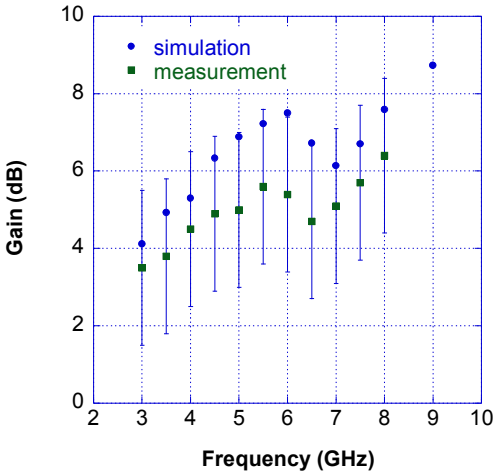

Fig. 12. Comparison between measured and simulated antenna gain.

Finally, by using the facilities available at ENEA Casaccia, the radiation pattern of the antenna has been measured at 4, 6, and 8 GHz.

Figure 13 shows a comparison between the measured and simulated radiation pattern on the x-y vertical plane at 6 GHz. Also in this case, a good agreement between measurements and simulations has been found.

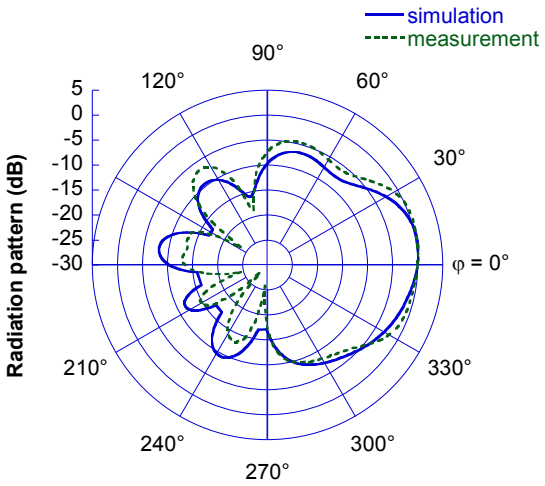

Fig. 13. Radiation pattern at 6 GHz.

V. CONCLUSION

The design of a fixed and a wearable planar UWB antenna usable in biomedical sensing of vital signs has been presented. Simulation results show that both antennas have a return loss better than -10 dB in the 3.1-10.6 GHz frequency band. Time domain performances of the fixed antenna have been investigated showing that it has a very good fidelity factor and an almost constant group delay. Moreover, it has been shown that with a suitable excitation of the wearable antenna it is possible to detect heart movements. Prototypes of the two antennas have been realized and return loss, gain, and radiation pattern have been measured, obtaining a good agreement between simulations and measurements.

VI. ACKNOWLEDGEMENTS

The authors wish to thank Dr. Paolo D'Atanasio and Mr. Alessandro Zambotti for their support during measurements carried out at ENEA-Casaccia.

REFERENCES

[1] E. M. Staderini, "UWB Radars in Medicine," *IEEE Aerospace and Electronic System Magazine*, vol. 17, no.1, pp. 13-18, Jan. 2002.

[2] S. Pisa, P. Bernardi, M. Cavagnaro, and E. Pittella, E. Piuzzi, "Monitoring of Cardio-Pulmonary Activity with UWB Radar: A Circuital Model," *Proc. Asia-Pacific Symp. on EMC & 19th Zurich Symp. on EMC.,* Singapore, pp. 224-227, May 2008.

[3] Federal Communications Commission, "New Public Safety Applications and Broadband Internet Access Among uses Envisioned by FCC Authorization of Ultra-Wideband Technology,"http://www.fcc.gov/Bureaus/Engineering_Technology/News_Releases/2000/nret0006.html, 2002.

[4] Federal Communications Commission, "45 CFR Part 15," http://www.fcc.gov/oet/info/rules, Revision of Part 15 of the Commission's Rules Regarding Ultra-Wideband Transmission, 2002.

[5] W. S. Chen and S. C. Wu "A Printed Heart Monopole Antenna with Band-Rejected Characteristics for IEEE 802.16a and UWB Applications," *Microwave Journal*, vol. 50, no. 5, pp.164, May 2007.

[6] A. M. Abbosh and M. E. Bialkowski, "Design of Ultrawideband Planar Monopole Antennas of Circular and Elliptical Shape," *IEEE Trans. Antennas Prop.*, vol. 56, no. 1, Jan. 2008.

[7] Y. Li et al., "A Novel Time-Domain UWB Antenna", *ICCS Singapore Int. Conf. on Comm. Systems,* pp. 793-796, Nov. 2008.

[8] S. Chamaani and S. A. Mirtaheri, "Planar UWB Monopole Antenna Optimization to Enhance Time-Domain Characteristics using PSO," *Int. J. Electron. Commun.*, AEU, 2008.

[9] H. Kanj and M. Popovic, "Two-Element T-Array for Cross-Polarized Breast Tumor Detection," *Applied Computational Electromagnetic Society (ACES) Journal*, vol. 23, no. 3, Sept. 2008.

[10] E. Gazit, "Improved Design of the Vivaldi Antenna," *IEE Proc., Part H*, vol. 135, no. 2, pp. 89–92, 1988.

[11] K. Yngvesson, T. Korzeniowski, Y. Kim, E. Kollberg, and J. Johansson, "The Tapered Slot Antenna - A New Integrated Element for Millimetre Wave Applications," *IEEE Microwave Theory Tech.*., vol. 37, no. 2, pp. 365–374, Feb. 1989.

[12] A. M. Abbosh, "Compact Antenna for Microwave Imaging Systems," *Proc. Biom. Eng. Conf. CIBEC'08,* 2008.

[13] CST Microwave Studio®, "Workflow and Solver Overview", CST Studio Suite™ 2008.

[14] D. Lamensdorf and L. Susma, "Baseband-Pulse-Antenna Techniques," *IEEE Ant. Prop. Magazine*, vol. 36, no. 1, February 1994.

[15] Z. N. Chen, X. H. Wu, H. F. Li, N. Yang, and Y. W. Chia, "Considerations for Source Pulses and Antennas in UWB Radio Systems," *IEEE Trans. Antennas Prop.*, vol. 52, no. 52, pp. 1739–1748, 2004.

[16] Q. Wu, R. Jin, J. Geng, and M. Ding, "Pulse Preserving Capabilities of Printed Circular Disk Monopole Antennas with Different Grounds for the Specified Input Signal Forms," *IEEE Trans. Antennas Prop.*, vol. 55, no. 10, Oct. 2007.

[17] Federal Communications Commission, "Evaluating Compliance with FCC Guidelines for Human Exposure to Radio Frequency Electromagnetic Fields," Supplement C to OET Bulletin 65 (Edition 97-01), Washington, DC 20554, 2001.

[18] K. S. Cole and R. H. Cole, "Dispersion and Absorption in Dielectrics. I. Alternating Current Characteristics," *J. Chem. Phys,* vol. 9, no. 4, pp. 341-51, 1941.

[19] S. Gabriel, R. W. Lau, and C. Gabriel: "The Dielectric Properties of Biological Tissues: III. Parametric Models for the Dielectric Spectrum of Tissues," *Phys. Med. Biol.,* vol. 41, pp. 2271–2293, 1996.

[20] http://niremf.ifac.cnr.it/docs/DIELECTRIC/AppendixC.html.

[21] H. Songoro, M. Vogel, and Z. Cendes, "Keeping Time with Maxwell's Equations," *IEEE Microwave Magazine,* vol. 11, pp. 42 – 49, April 2010.

[22] C. A. Balanis, "Antenna Theory: Analysis and Design," John Wiley & Sons, 2005.